Review

Fat and Water Magnetic Resonance Imaging

CME

Thorsten A. Bley, MD,[1,2] Oliver Wieben, PhD,[3,4] Christopher J. François, MD,[1] Jean H. Brittain, PhD,[5] and Scott B. Reeder, MD, PhD[1,3,4,6*]

A wide variety of fat suppression and water–fat separation methods are used to suppress fat signal and improve visualization of abnormalities. This article reviews the most commonly used techniques for fat suppression and fat–water imaging including 1) chemically selective fat suppression pulses "FAT-SAT"; 2) spatial-spectral pulses (water excitation); 3) short inversion time (TI) inversion recovery (STIR) imaging; 4) chemical shift based water–fat separation methods; and finally 5) fat suppression and balanced steady-state free precession (SSFP) sequences. The basic physical background of these techniques including their specific advantages and disadvantages is given and related to clinical applications. This enables the reader to understand the reasons why some fat suppression methods work better than others in specific clinical settings.

Key Words: fat and water MRI; fat suppression; spatial spectral pulses; STIR; chemical shift imaging; SSFP
J. Magn. Reson. Imaging 2010;31:4–18.

MOST CLINICAL magnetic resonance imaging (MRI) applications detect the signal from protons, which compromise over 90% of nuclei in the human body. The detected protons are either part of water, bound to molecules such as proteins or carbohydrates, or fat. Their respective signal intensities in imaging voxels results from a combination of their spin density, longitudinal and transverse relaxation times (T_1 and T_2, respectively), and the parameters of the imaging sequence used. By exploiting the particular characteristics of hydrogen atoms, MRI can provide excellent contrast between soft tissues, according to whether they are bound to water or to lipid molecules.

With its relatively short T_1 relaxation time, fat signal often appears bright in many important clinical imaging sequences and can obscure underlying pathology such as edema, inflammation, or enhancing tumors. For this reason, most clinical protocols use fat suppression methods to suppress fat signal and improve visualization of these abnormalities. This is particularly true for standard imaging sequences such as fast spin-echo (FSE), spoiled gradient echo (SPGR), and steady-state free precession (SSFP). Reliable fat-suppression has the added benefit of eliminating chemical shift artifact, by virtue of the fact that fat signal is no longer present, and lower bandwidths may be used with fat-suppressed applications to improve signal-to-noise ratio (SNR). In addition, there are several pathologies where direct visualization of fat may be desirable, such as fatty tumors, including adrenal adenomas, angiomyolipomas, liposarcomas, and other fat-containing mesenchymal tumors. There is also tremendous current interest in the quantification of the amount of visceral adipose tissue, as well as fatty infiltrative diseases such as hepatic steatosis (1–6). For any of these applications, separation of water and fat signals may be highly desirable with acquisition of "water-only" and/or "fat-only" images.

This article reviews the most commonly used techniques for fat suppression and fat–water imaging including 1) chemically selective fat suppression pulses "FAT-SAT"; 2) spatial-spectral pulses (water excitation); 3) short inversion time (TI) inversion recovery (STIR) imaging; 4) chemical shift based water–fat separation methods; and finally 5) fat suppression and balanced SSFP sequences (Table 1).

PHYSICS OF WATER–FAT IMAGING

NMR Spectrum of Water and Fat

The electronic shielding of the protons in the triglyceride molecules of fat is greater than that experienced by protons in water molecules, resulting in different microscopic magnetic fields, and subsequently different proton resonance frequencies. Fat has a complex spec-

[1]Department of Radiology, University of Wisconsin, Madison, Wisconsin, USA.
[2]Department of Diagnostic and Interventional Radiology, University Medical Center Hamburg-Eppendorf, Hamburg, Germany.
[3]Department of Medical Physics, University of Wisconsin, Madison, Wisconsin, USA.
[4]Department of Biomedical Engineering, University of Wisconsin, Madison, Wisconsin, USA.
[5]Global MR Applied Science Laboratory, GE Healthcare, Madison, Wisconsin, USA.
[6]Department of Medicine, University of Wisconsin, Madison, Wisconsin, USA.
*Address reprint requests to: S.B.R., 600 Highland Avenue, CSC E1/374, Madison, WI, 53792-3252. E-mail: sreeder@wisc.edu
Received October 30, 2008; Accepted July 6, 2009.
DOI 10.1002/jmri.21895
Published online in Wiley InterScience (www.interscience.wiley.com).

Table 1
Most Commonly Used Techniques for Fat Suppression and Fat-Water Imaging

Method	Advantages	Disadvantages	Suggested applications
Chemically selective fat suppression	• Versatile • Relatively fast • Applicable to most pulse sequences	• Sensitive to B_0 and B_1 inhomogeneities • Low sequence efficiency	• Most applications except: • Head and neck • Mediastinum • Extremities with metal implants
Spatial-spectral pulses, water excitation	• Insensitive to B_1 inhomogeneities • Versatile • Relatively fast • Practical to most pulse sequences except FSE	• Sensitive to B_0 inhomogeneities • Low sequence efficiency • Longer excitation pulses	• 3D imaging of cartilage in knee • Most applications except: • Head and neck • Mediastinum • Extremities
STIR	• Robust to B_0 and B_1 inhomogeneities • Reliable fat suppression	• Mixed contrast • Inherent T_1weighting • Only works with PD and T_2W • Low SNR efficiency • Suppresses short T_1 species and enhancing tissue after contrast	• Head and neck • Chest • Abdomen • Extremities • Large field of view • Inhomogeneous B_0 • T2/PD applications
Chemical shift based water-fat separation	• Robust fat saturation • Provides fat/water images • Allows recombined images • Corrects for chemical shift • Universal compatibility • Quantitative applications • High SNR efficiency	• Long scan times • More complex reconstruction	• Anywhere fat saturation and water excitation fail • Anywhere fat information/ quantification is needed • Hepatic steatosis • Adnexal masses
SSFP methods	• Rapid • High SNR • Bright fluid	• T_2/T_1 mixed contrast • Banding and flow artifacts from B_o inhomogeneities • "India Ink" artifact • Currently under development • Limited clinical experience	• NCE vascular imaging • Bowel imaging • New applications being explored

trum with multiple peaks, the largest of which is shifted downfield by ≈3.5 ppm from the water peak (Fig. 1). For simplicity and practicality, we will limit the majority of the discussions in this article to this single fat resonance peak, which usually contains more than 10 times the signal energy of any other fat peak (7). It is important to realize, however, that advanced quantitative applications may need to consider these additional peaks of fat.

The resulting chemical shift, Δf_{cs}, in the resonance frequency is linearly related to the magnetic field strength B_0:

$$\Delta f_{cs} = \frac{\gamma}{2\pi} B_0 \times \Delta\delta[\text{ppm}] \times 10^{-6} \qquad [1]$$

where γ is the gyromagnetic ratio and $\gamma/2\pi = 42.58$ MHz/T. At 1.5T, the resonance frequency for protons is ≈63.9 MHz. At body temperature the chemical shift between protons and fat is approximately −210 Hz (fat precesses more slowly than water) (8). As explicitly written in Eq. 1, the chemical shift is directly proportional to the main magnetic field B_0. Therefore, at 3.0T, an increasingly important clinical field strength, the chem-

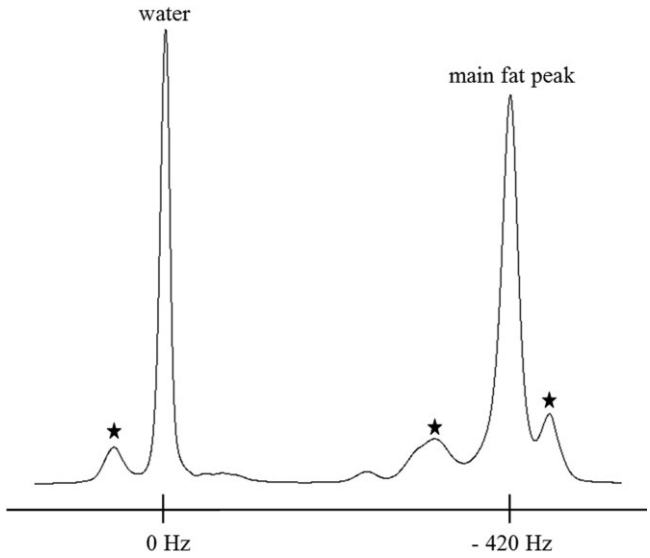

Figure 1. NMR spectrum of water–fat mixture acquired at 3T demonstrates a single resonance for water. The main fat peak resonates 420 Hz more slowly than the water (on resonance in this figure). It is important to note that fat actually has several additional peaks (*), some of which lie near the water resonance. For the purpose of this work, we will consider fat a single peak at −420 Hz at 3T (or −210 Hz at 1.5T).

ical shift between water and the main fat peak doubles to −420 Hz.

It is important to note that the resonance frequency of water is dependent on the temperature of the tissue being imaged, and therefore the apparent chemical shift between water and fat is dependent on the local temperature (9). For example, the chemical shift between water and the main fat peak is −210 Hz at body temperature, and −224 Hz at 22°C. These temperature differences may be important for specific fat suppression and water–fat separation applications in tissue or phantoms not at 37°C.

Main Magnetic Field (B_0) Inhomogeneities

Several of the fat–water separation techniques discussed below rely on the assumption that there are constant resonance frequencies for fat and water across the image. However, in practical applications many factors can create inhomogeneities in the main magnetic field (B_0) that violate this assumption and result in imperfect suppression of fat.

The main magnet itself may have an imperfect magnetic homogeneity, although this is usually a minor effect in modern MR scanners that are usually shimmed to homogeneity within 1 ppm across the field of view (FOV). Magnetic susceptibility introduced by the patient leads to more significant field distortions. For example, susceptibility differences at air/tissue interfaces such as the nasal cavities, ears, lungs, or skin can lead to large B_0 inhomogeneities. This also holds true for bowel gas and adjacent intraluminal fluid or ascites. Susceptibility differences, in general, are proportional to the main magnetic field, and therefore worsen at higher field strengths. Furthermore, implanted ferromagnetic objects such as dentures, surgical clips, staples, prosthetic joints, etc., may cause more severe distortions in the static magnetic field. The susceptibilities lead to geometrically dependent field inhomogeneities that shift the resonance frequencies of water and fat relative to the MR system's transmit and receive frequencies.

For traditional Cartesian applications (ie, spin-warp *k*-space sampling), B_0 inhomogeneities have three main effects: 1) distortion in the readout direction, 2) accelerated T_2* decay for gradient echo imaging, and 3) failed fat suppression, which is the most relevant for this article. As discussed in more detail below, field inhomogeneities shift the position of the water and fat peaks with respect to the frequency-selective profile of the fat-saturation pulse, resulting in failure of the desired fat suppression and possibly leading to inadvertent loss of water signal.

Radiofrequency (RF) (B_1) Inhomogeneities

Receive B_1 inhomogeneities can cause intensity variations across the image. However, these are infrequently a problem in clinical routine, and B_1 sensitivity correction algorithms are widely used and available on most modern scanners. Transmit B_1 inhomogeneities, however, lead to inhomogeneous flip angles across the image and can be problematic for some fat suppression methods. This problem is often minimized by using body or bird cage coils that provide a more homogenous transmit field in combination with (relatively inhomogeneous) receive phased arrays of surface coils. At 3.0T, dielectric effects can also lead to variations in the achieved flip angle, particularly in abdominal imaging applications and in the presence of ascites. Fortunately, advanced design techniques, such as adiabatic approaches, can generate RF pulses that are relatively insensitive to B_1 variations, addressing this concern for many applications.

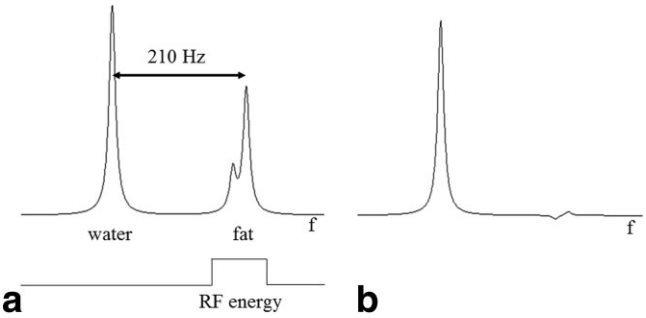

Figure 2. Schematic spectrum of water and fat peaks and the positioning of a spectrally selective "rect" function ("fat-sat pulse") with a particular bandwidth centered on the main fat peak, −210 Hz from the water peak at 1.5T, before (**A**) and after (**B**) the application of the fat-saturation pulse. RF energy = Fourier spectrum of the fat-saturation pulse.

CHEMICALLY SELECTIVE FAT SUPPRESSION PULSES "FAT-SAT"

In 1985 Haase et al (10) introduced a chemical shift selective (CHESS) imaging technique that can be used to selectively excite certain spin species such as fat or water, irrespective of their spatial location. Using this technique, the desired component of longitudinal magnetization (eg, water) remains unaffected while the unwanted component (eg, fat) is left with no net magnetization.

Typically, the saturation pulse carrier frequency is centered at the main fat peak and the RF amplitude envelope is designed as a "sinc" function or related function. In the Fourier (spectral) domain the RF sinc pulse becomes a "rect" function (which has a "rectangular" shape, hence the name) with a bandwidth determined by the width of the sinc lobes in such a way that it does not affect the water frequency. This leads to a rect function of RF energy at the location of the main fat peak (Fig. 2). If the flip angle of this pulse is adjusted to 90°, all longitudinal magnetization in the fat peak will be tipped into the transverse plane. In reality, the RF pulse is a truncated sinc and the spectral sensitivity is altered slightly from the idealized "rect" function. The RF pulse is followed by a crusher gradient to spoil this transverse magnetization, saturating all transverse magnetization of fat. Such fat-saturation pulses (chemically selective RF pulses and crusher gradients) are followed immediately by a standard imaging sequence. This leaves little time for recovery of fat longitudinal magnetization, resulting in suppression of signal from

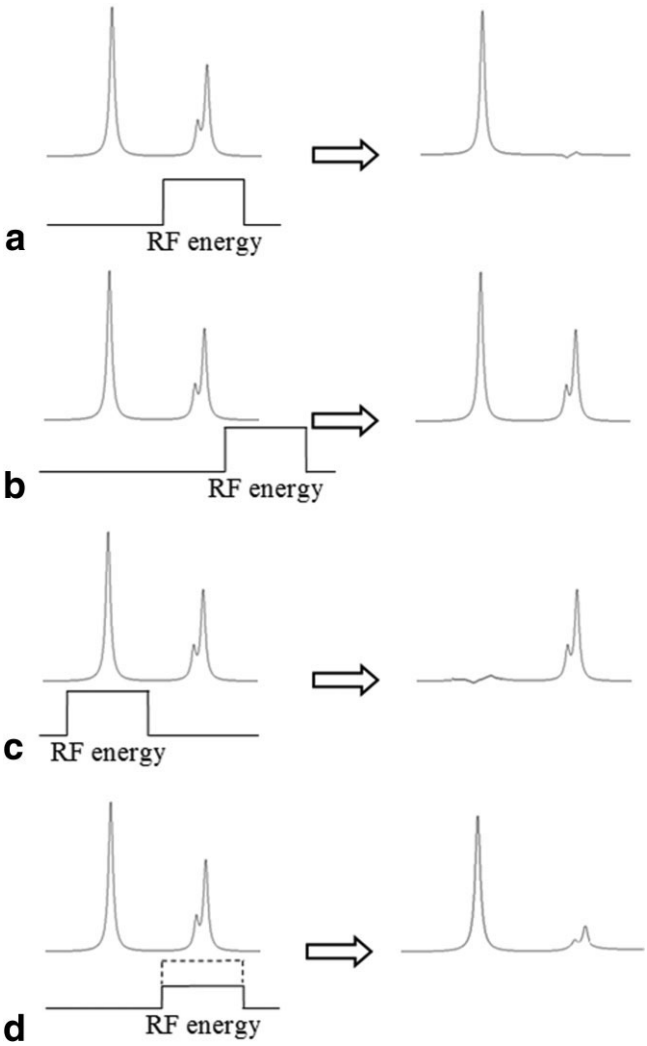

Figure 3. Schematic displaying the effect of B_0 and B_1 inhomogeneities on fat sat pulses. The rect pulse played for fat saturation placed correctly at the fat signal establishes the desired fat saturation (**A**). With B_0 inhomogeneities in the field the SINC pulse may result positive or negative to the fat water spectrum which may lead to missed or incomplete fat suppression (**B**) or inadvertent water suppression (**C**), respectively. Spatially varying flip angles across the FOV may lead to B_1 inhomogeneities that result in an insufficient fat sat pulse and thus lead to incompletely saturated fat signal (**D**).

fat-containing tissues. Fat saturation pulses are highly effective in regions where both the main magnetic field (B_0) and the transmit RF field (B_1) are relatively homogeneous (Fig. 3). Typical areas where fat-saturation pulses are effective include targeted volumes of the knee, pelvis, and abdomen. Fat-saturation is more challenging over large FOVs, in head and neck imaging, and in areas with metallic implants.

The primary disadvantage of fat-saturation pulses is that they are relatively sensitive to B_0 inhomogeneities that shift the position of the water and fat peaks with respect to the frequency of the fat-saturation pulse (Fig. 3B,C). This can result in failed fat suppression, and can even cause inadvertent suppression of water signal. Therefore, high-quality fat suppression with fat saturation pulses requires a relatively homogeneous magnetic field over the entire FOV, to allow the lipid protons to resonate at the same frequency throughout the imaging volume. Even with optimal shimming, magnetic susceptibility variations in the patient may impair the quality of fat suppression.

Furthermore, fat-saturation pulses are sensitive to B_1 inhomogeneities, because robust fat-saturation requires a relatively accurate 90° pulse (that can typically be achieved within ≈5–10° degrees) in order to saturate the longitudinal magnetization of fat (Fig. 3D). A 45° pulse, for example, would provide only partial suppression of fat. Typical and acceptable levels for B_0-uniformity are approximately <1 ppm. Since the signal of all lipid protons needs to be saturated without affecting the water signal, fat sat does not perform well with transmit surface coils. Coils with uniform RF fields, such as head, body, and extremity coils are preferred.

At higher field strengths the chemical shift increases between water and fat. At 3.0T, for example, the chemical shift of the fat and water spectrum is approximately −420 Hz. In principal, field variations due to susceptibility should also double, proportional to the main magnetic field, which will widen the distribution of magnetic field inhomogeneities. One might expect the increased susceptibility to offset the increased chemical shift between water and fat, and there should be no overall improvement in the performance of fat suppression at higher field strengths. In practice, however, fat suppression performs better at higher field strengths and it is easier to suppress the fat signal without affecting the water signal. This may be due to the fact that a wider spectral bandwidth of RF energy is used to suppress fat, which requires shorter RF pulses in the time domain. Shorter RF pulses generally perform better and are easier to design, and this may result in overall improved fat suppression. Following the same logic at lower field strengths, where the chemical shift between the water and fat signals is reduced, longer RF pulses are needed to obtain a good spectral profile. Tradeoffs are necessary to minimize the duration of the RF pulses and performance can be degraded relative to higher field strengths, with an increased opportunity for failed fat suppression and/or suppressed water signal.

SPATIAL-SPECTRAL PULSES (WATER EXCITATION)

A more advanced approach for fat suppression is to excite the water peak directly, rather than suppress the fat peak (11,12). One of the earliest implementations, known as "spatial-spectral" pulses, invoked the concept of adding a spectral dimension to excitation *k*-space (11). Spatial-spectral pulses are unique in that they simultaneously excite a spatial region of spins (eg, a slice) as well as a spectral band (eg, water) in order to provide excitation of the water signal only within the slice of interest.

The mechanism behind spatial-spectral pulses can be explained in a simplified manner as follows. Consider a train of slice-selective "α" pulses, each with a small tip angle, α, eg, 5–10°. These α pulses are separated by the time needed for fat to precess 180° relative

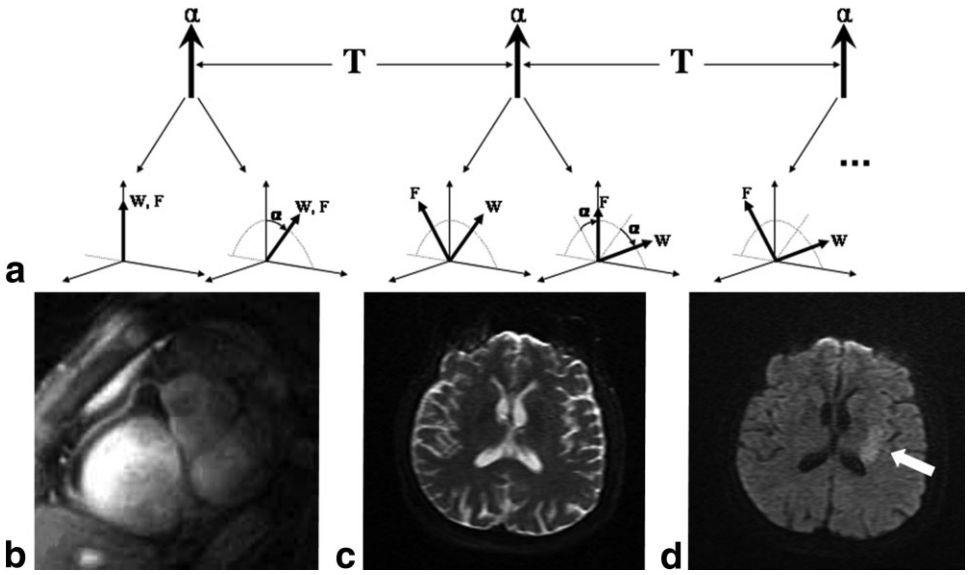

Figure 4. Schematic of spatial-spectral pulses. **A:** α pulses are separated by a time, T, sufficient to create a 180° phase shift between water and fat. T is ≈2.3 msec at 1.5T. Immediately after the first α pulse, water and fat are tipped together. However, immediately before the next α pulse the fat has precessed 180° such that after the second α pulse, the fat is tipped back up along the M_z axis and the water is tipped further toward the transverse plane. 3.0T cardiac MR utilizing spatial-spectral imaging of the right coronary artery suppresses the surrounding fat tissue in the right atrioventricular groove (**B**). Image courtesy Krishna Nayak, PhD (Department of Electrical Engineering, University of Southern California, Los Angeles). Using spatial-spectral pulses all fat in the subcutaneous tissue has been effectively suppressed in a 70-year-old woman with left MCA infarct. Restricted diffusion can be readily revealed on the EPI image with a *b*-value of 0 mm^2/s (**C**) and 1000 mm^2/s (arrow in **D**).

to water, or $T = 1/(2\Delta f)$, about 2.3 msec at 1.5T. After the first α pulse, both fat and water are tipped α degree from the *z*-axis. Immediately before the next pulse, however, the fat has precessed 180° in the transverse plane, and is subsequently tipped back along the M_z axis, while the water continues its trajectory toward the transverse plane (Fig. 4). In this way the water resonance is selectively excited, while the fat resonance remains unaffected. Details of spatial-spectral pulses have been described in greater detail elsewhere (11).

Spatial-spectral pulses are a very effective means of selectively exciting water within an image and are most commonly used in conjunction with spiral and echo planar imaging (EPI) (13,14) (Fig. 4C,D). They can also be combined with other sequences such as spoiled gradient echo and fast spin-echo imaging (15,16). The major drawback of spatial-spectral pulses are their sensitivity to B_0 inhomogeneities, which is similar to conventional fat-saturation pulses (11,14). The other major drawback is the need for relatively lengthy pulses, which can reduce overall sequence efficiency. For this reason spatial-spectral pulses are most commonly used with sequences requiring only a few excitations and longer TRs.

Binomial water excitation pulses have been proven to be beneficial for cartilage imaging (17), where uniform fat suppression with high spatial resolution is required. Cartilage imaging with single frequency selective RF pulses at ultrahigh-fields has been shown to be easily applicable for fat suppression or fat–water separation (18).

An advantage of spatial-spectral pulses compared to fat-saturation pulses is that they are relatively insensitive to B_1 inhomogeneity because they directly excite the water signal, and avoid incomplete fat suppression associated with fat-saturation pulses that require uniform RF flip angles across the sample.

Spatial-spectral pulses work particularly well at higher field strengths because shorter RF pulses can be used, which facilitates a wider spectral bandwidth of RF energy centered at the main fat peak, making fat saturation less sensitive to B_0 inhomogeneities. Shorter pulses can be achieved because there is increased frequency separation between the water and fat resonances. This allows a shorter time between the multiple excitation pulses, as shown by time period "T" in Fig. 4A. For example, 3.0T cardiac MR utilizing spatial-spectral imaging in healthy volunteers has been shown to result in improved image quality, improved blood SNR efficiency, and significant improvement in blood-myocardium contrast-to-noise ratio (CNR) efficiency compared to 1.5T. Taking full advantage of the gradient and RF capabilities the spatial-spectral excitation duration was as short as 3.6 msec (19). Figure 4B shows a clinical example of the right coronary artery acquired at 3T using this technique. Figure 4C,D show examples of spatial-spectral excitations in combination with diffusion-weighted imaging in the brain. This approach is used by most EPI methods.

SHORT TI INVERSION RECOVERY (STIR)

Inversion recovery (IR) pulses are known to produce heavily T_1-weighted images. With the use of higher magnetic field strength which evolved in the 1980s, the tissue T_1 increased and a longer time was required to

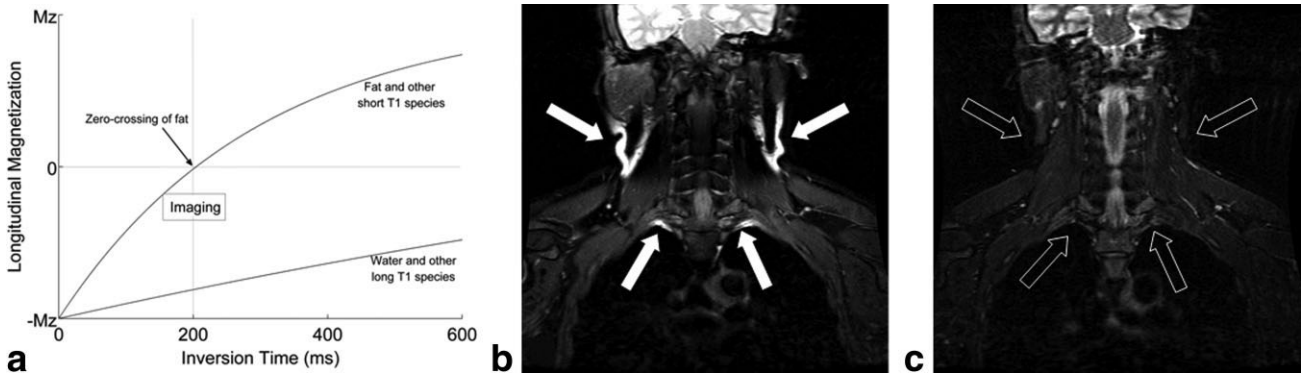

Figure 5. Schematic displaying the longitudinal magnetization of fat and water in relation to the inversion pulse (**A**). T_1 of fat is shorter than T_1 of water tissue. Short TI inversion recovery imaging acquires images ≈200 msec after the inversion pulse, during the fat zero-crossing (fat is nulled at this time), providing robust fat suppression, but less SNR performance. Insufficient fat suppression occurred in the cervical subcutaneous fat and at apex of the lungs (arrows in **B**) in T_2-weighted fat saturated fast spin echo (B). Homogenous fat suppression was achieved in the corresponding STIR images (light arrows in **C**). Note mixed contrast displayed in the depicted part of the brain in the STIR image.

produce equivalent image contrast with IR sequences. In the mid 1980s Bydder et al (20,21) introduced an important variant of the conventional IR sequence in which the initial inversion pulse was timed in a way that the signal from fat (short T_1) was nulled. This "short TI inversion-recovery" (STIR) method suppresses the signal of tissues with short T_1 values such as fat. STIR imaging has been used to increase the contrast between tumor and surrounding normal tissues mainly by nulling the fat signal (21). However, STIR images also introduce unwanted T_1 contrast into the remaining water signal, which may be a confounding factor when interpreting STIR images. Due to the risk of nulling contrast enhancing tissue, STIR imaging is used primarily for T_2 and proton density (PD) weighted imaging, and T_1 weighted STIR imaging should be avoided especially when using extrinsic contrast agents. Utilizing IR imaging, the signal intensity of any tissue can be nulled by variations in the inversion time (TI) (22). By choosing a short inversion time, the short T_1 tissue signal is suppressed (Fig. 5A). The TI corresponding to fat signal suppression in STIR is ≈100–200 msec at 1.5T as compared to 1500–2500 msec for the long-TI fluid attenuated inversion recovery sequence (FLAIR) for brain imaging. In general the TI should be increased when imaging at 3.0T due to the longer T_1 of tissue at higher field strengths.

The primary advantage of the STIR pulse sequence lies in its ability to produce uniform fat suppression. Even in difficult areas of the body the STIR sequence has proven to be extremely reliable, with strong insensitivity to B_0 inhomogeneities (Fig. 5B,C). Furthermore, respiratory artifacts are less pronounced and confusion with intraabdominal fat can be avoided, allowing bowel loops to be reliably identified (20).

Disadvantages of STIR pulses include the inherent T_1-weighting that limits its use to T_2-weighted imaging or proton density-weighted imaging. It is also relatively inefficient, requiring an inversion time of ≈200 msec. The inversion also degrades the SNR of the remaining water signal by ≈40%–50%. Practically, STIR is only used with fast spin-echo or spin-echo techniques. Even though it is insensitive to B_0 inhomogeneities, it may be sensitive to B_1 inhomogeneities if the inversion pulse is not an adiabatic pulse, particularly at higher field strengths, where B_1 may be more inhomogeneous.

It is important to stress that the inversion pulse and subsequent recovery of longitudinal magnetization alters the image contrast. Because gadolinium reduces the relaxation time T_1, the signal from gadolinium-enhancing lesions may be inadvertently suppressed. Therefore, T_1-weighted STIR imaging should always be avoided, particularly with contrast-enhanced imaging. However, since STIR sequences provide excellent fat suppression over large FOVs while being very insensitive to B_0 inhomogeneities, it is clinically a very practical method and is widely used.

CHEMICAL SHIFT BASED WATER–FAT SEPARATION METHODS

Chemical shift based water–fat separation methods comprise a class of approaches commonly known as "Dixon" water–fat separation (8,23–26). Unlike the methods described above, which suppress fat signal or selectively excite water, Dixon methods rely on the phase shifts created by fat–water resonance frequency differences to separate water from fat. Phase information is encoded by acquiring images at slightly different echo times (TE), exploiting the difference in resonance frequency between water and fat. By strategically acquiring images at specific TE values, the combined signal from a voxel containing water and fat signals can be decomposed into separate water and fat images. In this way, Dixon methods provide a "fat-suppressed" water-only image and a "water-suppressed" fat-only image. This approach was first proposed by Dixon (23), with two images acquired at different TEs such that water and fat were "in-phase" (S_{in} = W+F) or "out of phase" (S_{out} = W–F). By adding and subtracting S_{in} and S_{out}, water (W) and fat (F) images are easily separated, since $W = (S_{in} + S_{out})/2$, and $F = (S_{in} - S_{out})/2$, (Fig. 6). The original approach required only two images, thus it was considered a "two-point" method.

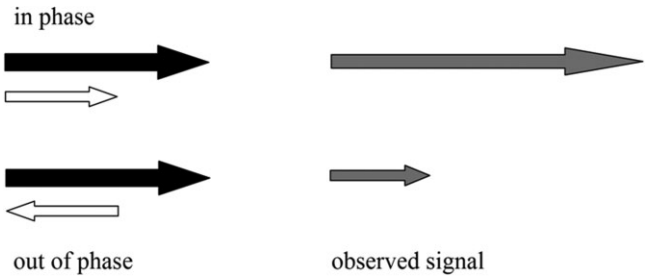

Figure 6. Signal vector diagram describing the conventional Dixon method. The signal of water (W) and fat (F) is added and the resultant signal is observed. Water and fat images can be generated by adding and subtracting the "in phase" (upper row) and the "out of phase" images, respectively (lower row).

Unfortunately, Dixon's original approach was sensitive to B_0 inhomogeneities that resulted in water–fat "swapping" in the image. As discussed below, this occurs because B_0 inhomogeneities create a natural ambiguity when only one chemical species (water, fat) dominates the signal from the pixel: fat signal is indistinguishable from water signal that is off-resonance by −210 Hz, etc. Unwrapping algorithms are needed to avoid this ambiguity.

The Dixon two-point method was subsequently modified by Glover and Schneider (24), by acquiring a third image that was used to compensate for B_0 inhomogeneities. This "three-point" approach acquired images at TE values that generated phase shifts of 0, $+\pi$, and $-\pi$ between the water and fat (24). The additional information can be used to calculate a B_0 field inhomogeneity image ("field map"). By using phase unwrapping algorithms, this approach can remove the effects of the field map, thereby avoiding fat–water swapping. By addressing the problems involved with B_0 inhomogeneity this technique became a more robust method, particularly at areas of high susceptibility. Glover (27) also suggested a four-point method with phase shifts of 0, π, 2π, and 3π and an additional measurement of the spectral width of the fat resonance.

Dixon methods are also insensitive to B_1 inhomogeneities and provide robust water–fat separation. They are compatible with a wide variety of pulse sequences including T_2-weighted FSE, T_1-weighted FSE, gradient echo, and SSFP. Fat-saturation typically fails in certain regions of the body because of unfavorable geometry, eg, in the lung apices and in the neck where large susceptibility differences create severe magnetic field inhomogeneities. Chemical shift methods are more robust in these areas (Fig. 7). In addition to the water-only images, fat images and recombined in-phase and out-of-phase images are also available for review using these water–fat separation methods. Importantly, chemical shift artifact, which causes a spatial shift of fat signal in the readout direction, can be removed by realigning the separated water and fat images before recombination to form these synthesized in-phase and out-of-phase images (28). This opens interesting possibilities for improved SNR performance through low-bandwidth imaging, free from chemical shift artifact. This is particularly true at higher field strengths, where relatively high bandwidths are typically used to avoid chemical shift artifact.

The primary disadvantage of Dixon methods is the increased scan time. Despite this, these methods are generally highly SNR-efficient if the correct choice of TEs are used (29). With the correct choice of echoes, the signal from the three images can achieve the maximum possible SNR in the water and fat images. Methods for scan time reduction have been investigated through partial *k*-space acquisition methods and parallel imaging (30,31). The latter approach is highly complementary with Dixon methods, because SNR penalties of parallel imaging are offset by gains in the SNR from the Dixon reconstruction when using well-defined phased array coils and optimized parallel imaging algorithms that minimize local noise amplification (g-factor) (30).

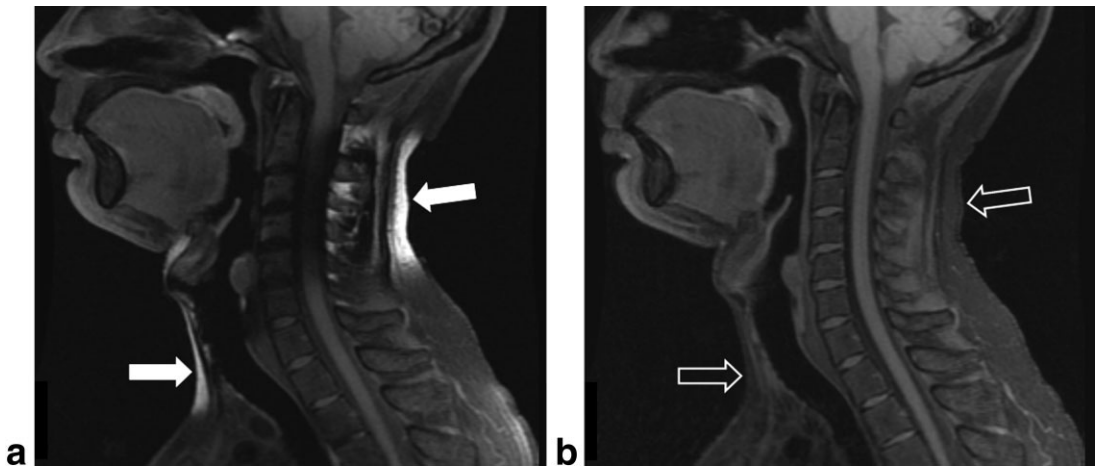

Figure 7. Sagittal T_1W-FSE images of the cervical spine utilizing conventional fat-saturation method (**A**) and Dixon imaging (**B**). Fat suppression failures of the subcutaneous fat at the anterior and posterior aspect of the neck in areas of air/tissue interfaces are present with the conventional fat-saturation method (arrows in A). Utilizing Dixon imaging a homogenous suppression of fat can be readily appreciated in the same patient as in A. Note that even in the areas of air/tissue interfaces homogenous fat suppression is achieved (arrows in B).

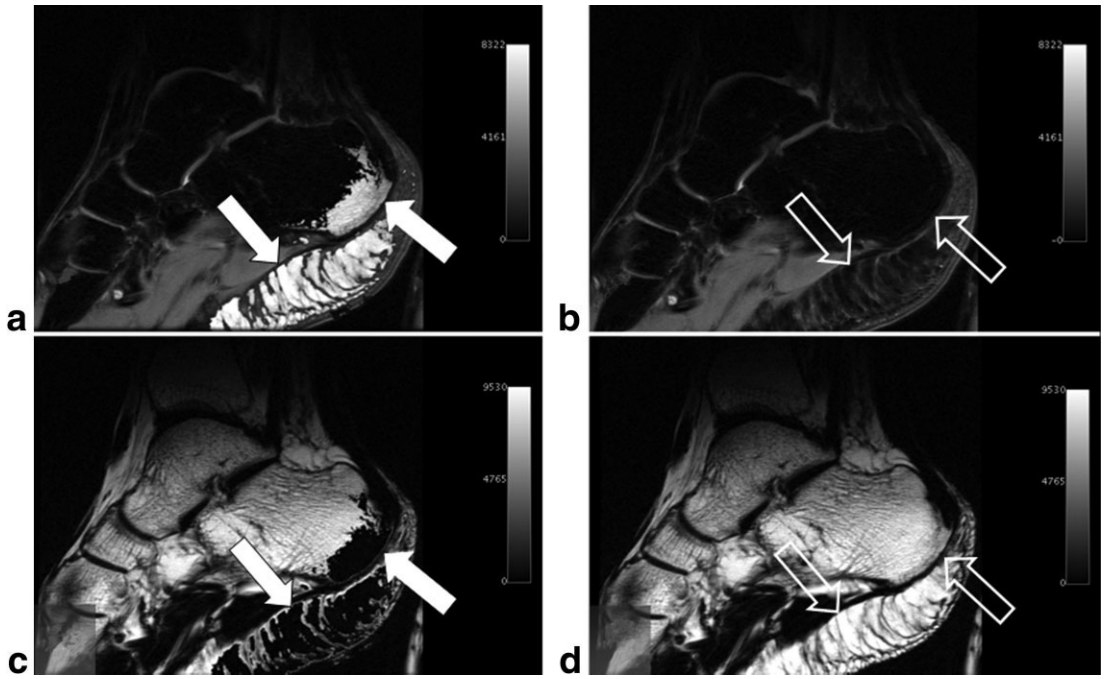

Figure 8. Sagittal water images (**A,B**) and fat images (**C,D**) of a foot demonstrate "water–fat swapping" (arrows in A,C). "Water–fat swapping" can be avoided by utilizing reconstruction algorithms with region growing methods that take the field inhomogeneity into account (light arrows in B,D).

Inherent to all Dixon water–fat separation methods is a natural ambiguity that leads to "water–fat swapping" (Fig. 8). This occurs because a voxel containing only water (fat) "looks" like fat (water) that is off-resonance by −210 Hz (+210 Hz), at 1.5T. To solve this ambiguity, additional information is needed for region-growing reconstruction algorithms to avoid this swapping. Most unwrapping algorithms exploit the fact that B_0 field inhomogeneities vary smoothly across the image and are continuous. Sophisticated algorithms are needed to avoid these swaps, and most reconstruction algorithms use a variety of phase unwrapping approaches (24,32,33) or region-growing methods that estimate the correct field inhomogeneity map (34,35). The success of a water–fat separation method largely depends on its ability to avoid water–fat swaps.

Over the past decade, several methods have been proposed to improve on the methods proposed by Dixon and Glover. Xiang and An (8) proposed a three-point method which included a general direct phase encoding

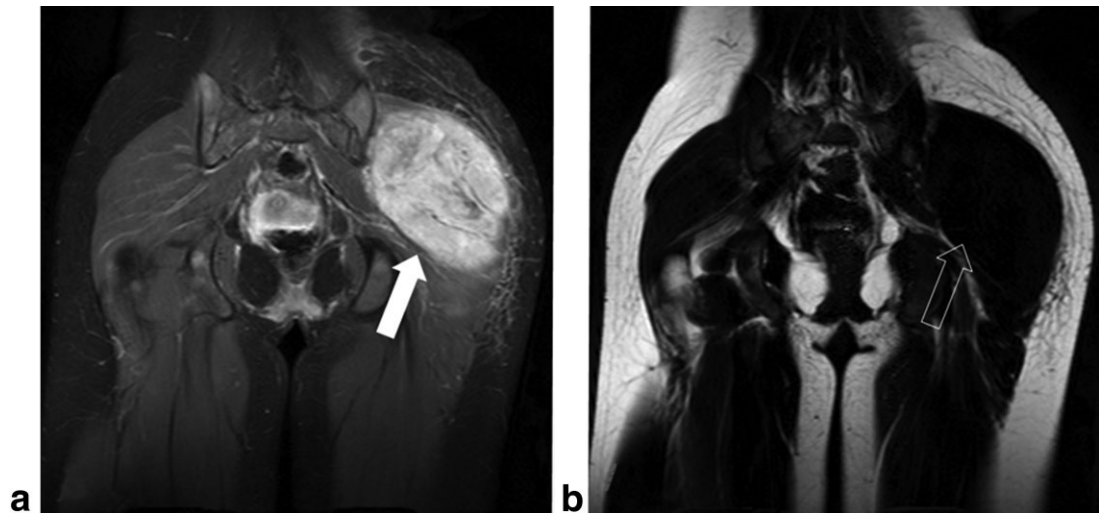

Figure 9. Large enhancing soft tissue mass in the left gluteal muscles after administration of gadolinium contrast, imaged with the three-point direct phase encoding method of Xiang et al. Uniform separation of water and fat is demonstrated. Selected acquisition parameters include: 1.5T, spin-echo, TR/TE = 800/24 msec, body coil. Images courtesy Q.S. Xiang, PhD (University of British Columbia, Vancouver, BC).

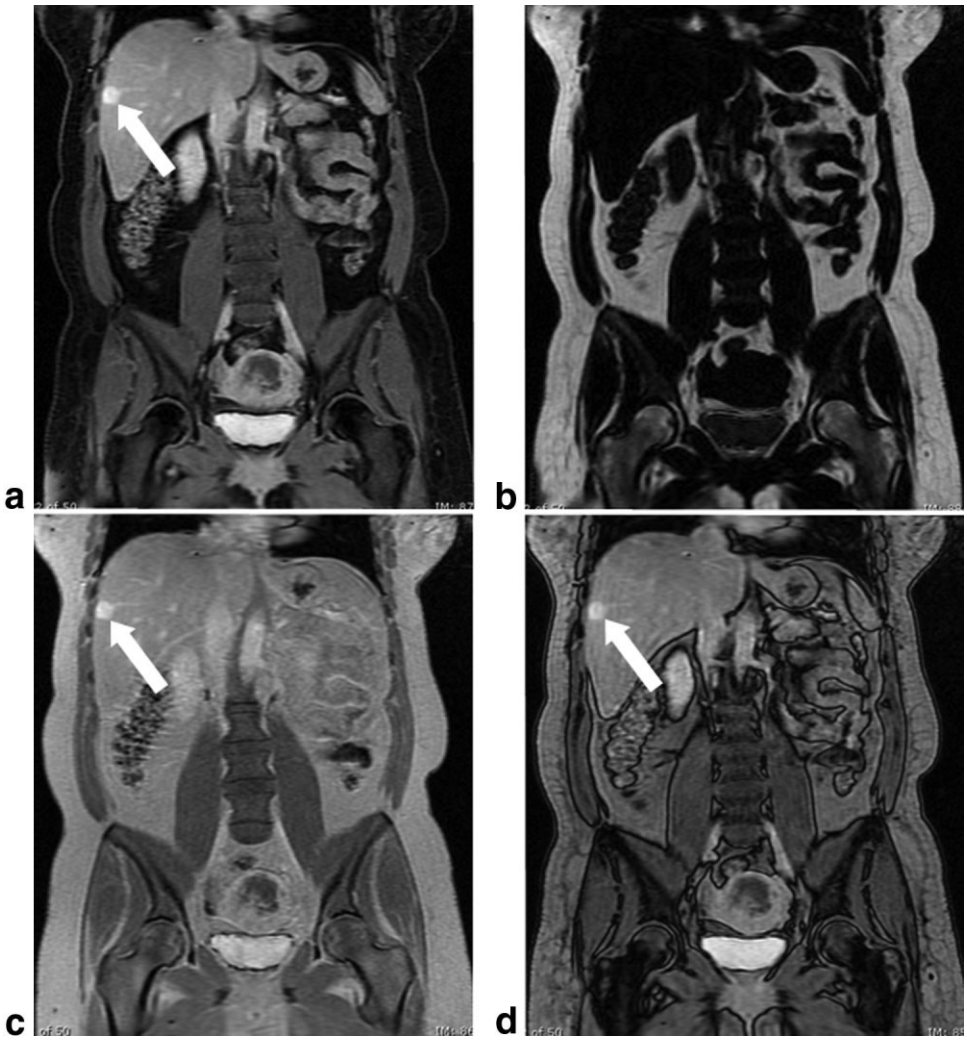

Figure 10. Uniform fat–water separation is achieved with a rapid contrast enhanced spoiled gradient acquisition using the z-point method described by Ma for robust fat–water separation over a large FOV. Excellent depiction of hemangioma is noted in the liver (arrow in **A,C,D**). A = water image, B = fat image, C = in-phase, and D = opposed-phase. Images courtesy Russell Low, MD (Sharps Children's Hospital, San Diego, CA).

(DPE) of the chemical shift information in 1997. A general asymmetric sampling scheme allowed an analytical solution for pixel-level water–fat separation using a region-growing method, rather than phase unwrapping, which can be challenging. A clinical example using the DPE approach is shown in Fig. 9. More recently, Xiang (36) reported an efficient and robust asymmetric two-point Dixon method with a partially opposed phase (POP) acquisition.

In 2002 Ma et al (25) introduced an FSE-based Dixon method that achieves an echo shift without requiring an increase in echo spacing, collects generally asymmetric echoes, and includes a phase-sensitive partial Fourier image reconstruction. In order to further decrease imaging time, Ma et al (37) then proposed a fast spin echo two-point Dixon method (fast 2PD) that uses two interleaved FSE images.

In 2004 Ma (32) also presented a novel phase correction algorithm that was based on a fast gradient echo sequence. This method applies a region-growing scheme that uses precalculated spatial gradients of the signal phase to guide the growth sequence and thus avoids manual selection of the seeds or usage of an empirical angular threshold. With this technique the signal direction of a given pixel is determined by the amplitude and phase of the surrounding pixels, whose direction has already been determined. This has proven to be very computationally efficient and robust, even in pixels with large phase uncertainty (Fig. 10) (38).

Iterative decomposition of water and fat with echo asymmetry and least squares estimation (IDEAL) is a multi-point water–fat separation method that has also been recently described (5,29,39–45) (Fig. 11). This technique allows for three or more echoes at arbitrary echo times that can be subsequently optimized to maximize the SNR performance of the water–fat separation. The optimal echo times, expressed in terms of the relative phase shift between water and fat, have been investigated both theoretically (46) and experimentally (29). In this work, it was shown that for a three-point acquisition, the center echo should have a phase between water and fat that is in quadrature (ie, perpendicular) in the first and third echo or subsequently $2/3\pi$ before and after the center echo, respectively. This gives an effective signal averaging of 3.0 for all combinations of water and fat, and therefore it is highly SNR-efficient, achieving the best possible SNR performance of the water–fat separation (Fig. 12). Reeder et al (29,43) showed that symmetrically acquired echoes lead to artifacts at water–fat tissue interfaces resulting from SNR

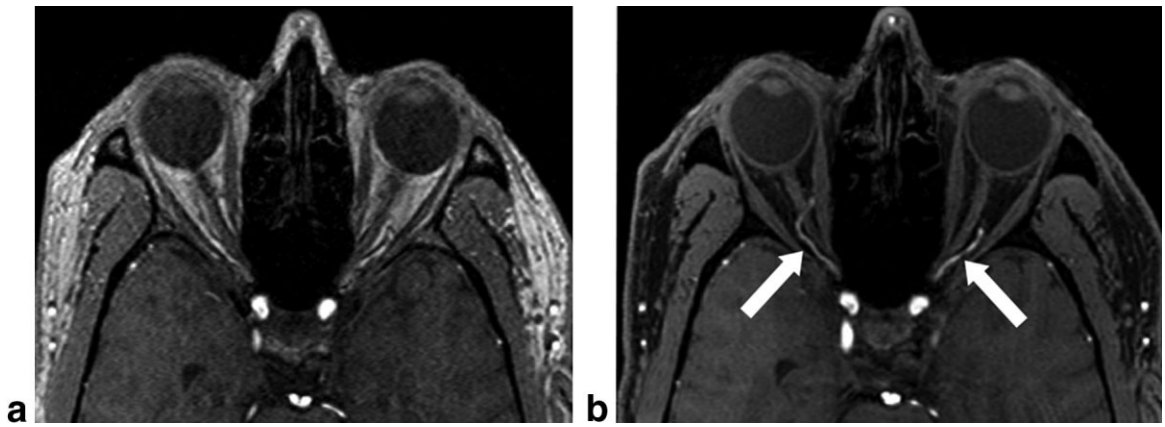

Figure 11. Conventional time of flight imaging with flow compensation fails to depict the ophthalmic arteries (**A**). Both ophthalmic arteries can be readily revealed by IDEAL time of flight imaging (arrows in **B**). As in the previous figure the fat signal is entirely eliminated and appears black rather than hypointense as seen with suppression methods.

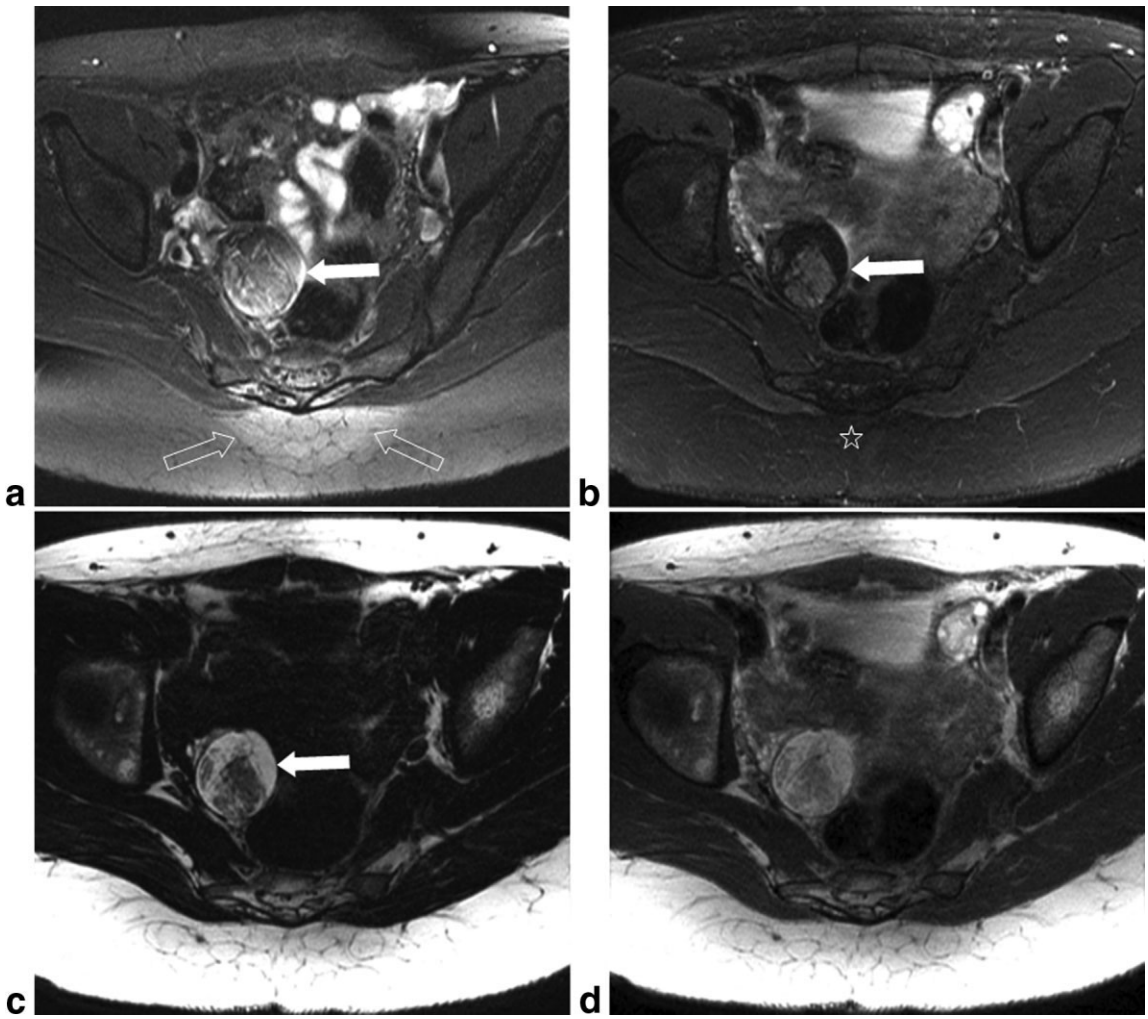

Figure 12. Transversal T_2-weighted, fat-saturated TSE of the pelvis of a 28-year-old woman with ovarian teratoma. Note failed fat suppression in the sacrum and dorsal subcutaneous fat (light arrows in **A**) and within the teratoma (arrow in A) due to lumbar metallic fixation rods cranial to the imaging plane. The water image of a T_2-weighted IDEAL fat-sat reveals homogeneous fat suppression in the respective location (asterisk in **B**). The ovarian teratoma is readily visualized on the water-image (arrow in B), the fat-image (arrow in **C**), and the in-phase-image (arrow in **D**). In fact, direct visualization of the fatty components within the teratoma is feasible in the water-image (arrow in B).

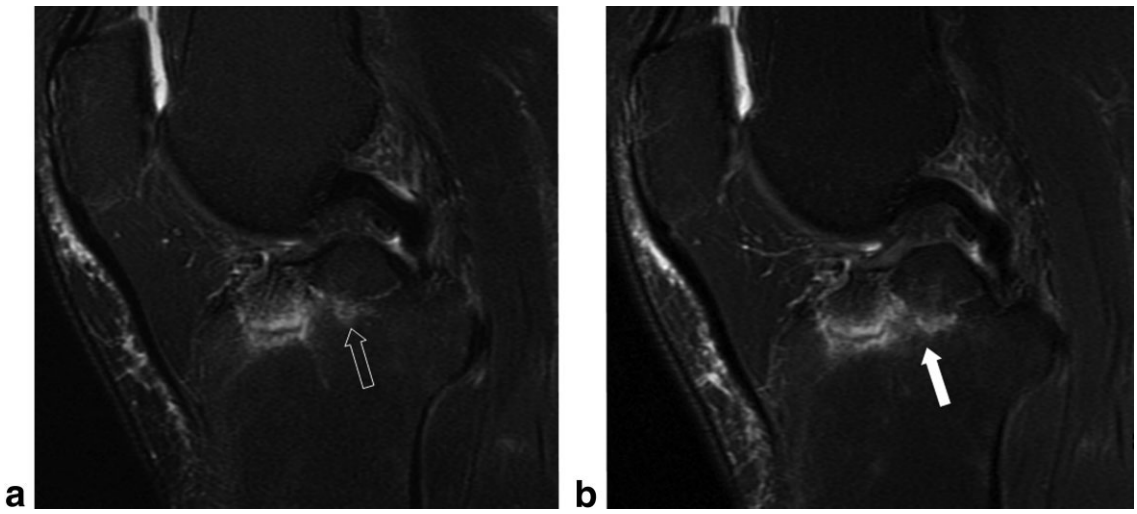

Figure 13. Sagittal T_2-weighted fat-saturated FSE sequence of the knee of a 56-year-old man with tibial plateau fracture. Note how extent of the bone marrow edema thins out toward the posterior portion of the tibial plateau on the fat sat FSE sequence (light arrow in **A**), while it is readily revealed on the IDEAL image with multipeak reconstruction (arrow in **B**).

performance that depended on the amount of water and fat in the voxel. The main disadvantage of IDEAL, like other three-point Dixon methods, is that it triples the scan time. Methods to reduce the scan time penalty include partial *k*-space acquisition (39,47), parallel imaging (48,49), and multiecho acquisition (50). An important advantage of the IDEAL method is that it can be modified to separate more than two species that have widely spaced resonance peaks, eg, fat-water-silicone (26,51), or ^{13}C labeled compounds (52,53).

Finally, IDEAL has the important advantage that the signal model can be easily modified to include multiple spectral peaks of fat (54) (Fig. 13). If the resonance frequencies and relative amplitudes of these peaks are known a priori, their contributions to the total fat signal can be more accurately modeled than a single resonance peak. This was recently shown to improve the quality of fat suppression, avoiding residual "gray" fat that results from incomplete separation of water and fat (54). As described below, accurate spectral modeling of fat has also been shown to improve the accuracy of water–fat separation methods that attempt to quantify fat (55,56).

The description of chemical shift based water–fat separation methods given above is certainly not complete. A more detailed discussion would be beyond the scope of this article and is found elsewhere in the literature (58).

FAT SUPPRESSION AND BALANCED SSFP

In the past 7–8 years, there has been considerable effort placed on new fat suppression methods with SSFP. SSFP is a rapid pulse sequence with very high SNR performance, and is commonly used for cardiac and abdominal imaging. SSFP has a mixed contrast that depends on the ratio of T_2/T_1, such that fat appears very bright, and robust fat suppression with SSFP is highly desirable.

The interesting phase behavior of SSFP with nonuniform spectral response allows an opportunity to develop new fat suppression methods unique to this sequence. As shown in Fig. 14, SSFP exhibits a repeating "passband" behavior with periodic magnitude and phase behavior at different off-resonance frequencies (58–60). The period of the passbands is equal to 1/TR, which is the time needed for an off-resonance spin to nutate by 360°. Importantly, the phase of adjacent passbands will alternate between 0 and 180° (ie, the sign of the transverse magnetization alternates between plus and minus), when TE = TR/2, which is the most commonly used TE for SSFP acquisitions. If water and fat resonances fall within adjacent passbands then this will create opposing phase of the water and fat.

The opposing phase created by the phase behavior of the SSFP signal will result in the familiar "India ink" artifact that occurs at water–fat interfaces, commonly seen in SSFP images. This occurs because of destructive interference of water and fat signals through a partial volume effect, when water and fat resonances fall in different passbands. It is important to realize that this effect is not a constant feature of SSFP images and only occurs when water and fat resonances fall within passbands that have opposite phase. Changes in the TR or in the field strength may result in the water and fat peaks having the same phase (0° or 360°), will lead to addition of the water and fat signal, and the India artifact at the water–fat interface will no longer be present. Figure 14 shows an example of this effect in cardiac images acquired at 3.0T with different TR values, resulting in variable behavior of the India ink artifact. A schematic of the magnitude (Fig. 14C, top) and phase behavior (Fig. 14C, bottom) of the SSFP signal response is plotted against the phase developed by a spin during one TR. This complex phase behavior of SSFP can also be exploited to separate water and fat, and several approaches have been described. A linear combination SSFP technique which is able to generate spectral se-

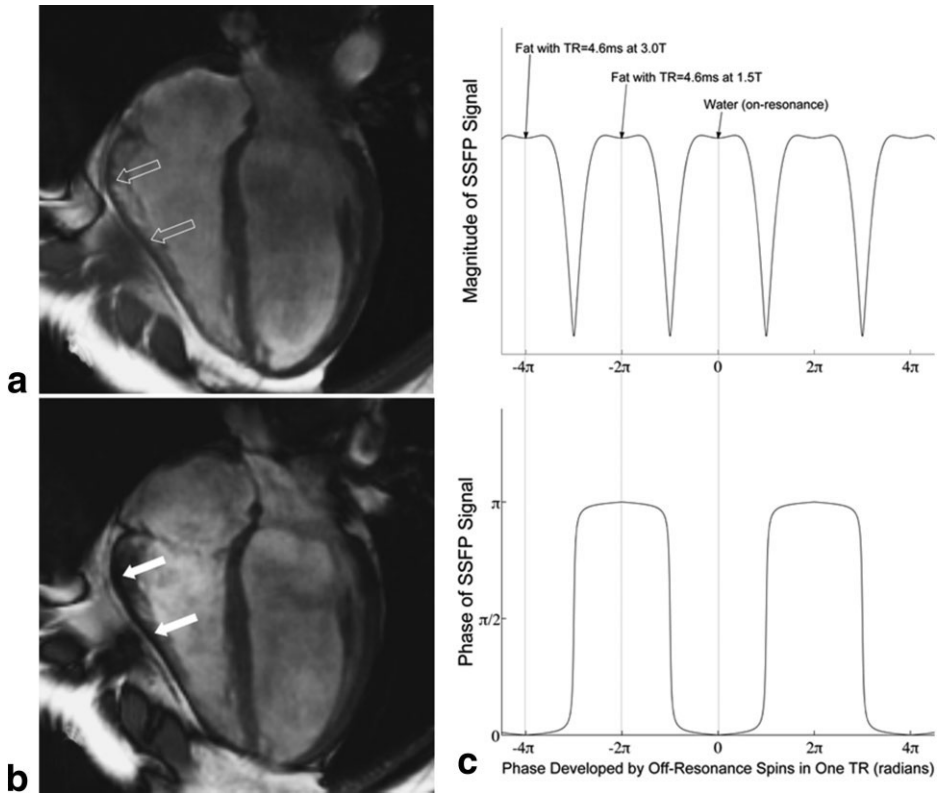

Figure 14. Four-chamber view SSFP cardiac MRI without (light arrows in **A**) and with "India-ink" artifact at fat-water interfaces (arrows in **B**). Schematic of the magnitude and phase of the SSFP signal response plotted against the phase developed by a spin during one TR, resulting from off-resonance effects such as B_0 inhomogeneity and/or chemical shift from fat (**C**). For example, with a TR of 4.6 msec the passbands are separated by −210 Hz. On-resonance water spins would sit at 0 Hz in the central passband, while fat spins would fall exactly one passband to the left, with opposite phase of water. This leads to subtraction of water and fat signals in voxels containing both species, explaining the India-ink artifact at fat-water interfaces from partial volume effects and the phase behavior of SSFP (B). At different values of TR or at 3T, and in the presence of a magnetic field inhomogeneity, the relative positions of water and fat may fall into the same passband. In these situations the India ink artifact may not be present (A).

lectivity for water/lipid discrimination has been described for various clinical applications (62,63). They also introduced a fast, spectrally selective imaging method called fluctuating equilibrium magnetic resonance (FEMR), which permits simultaneous acquisition of several images with different contrast features. This

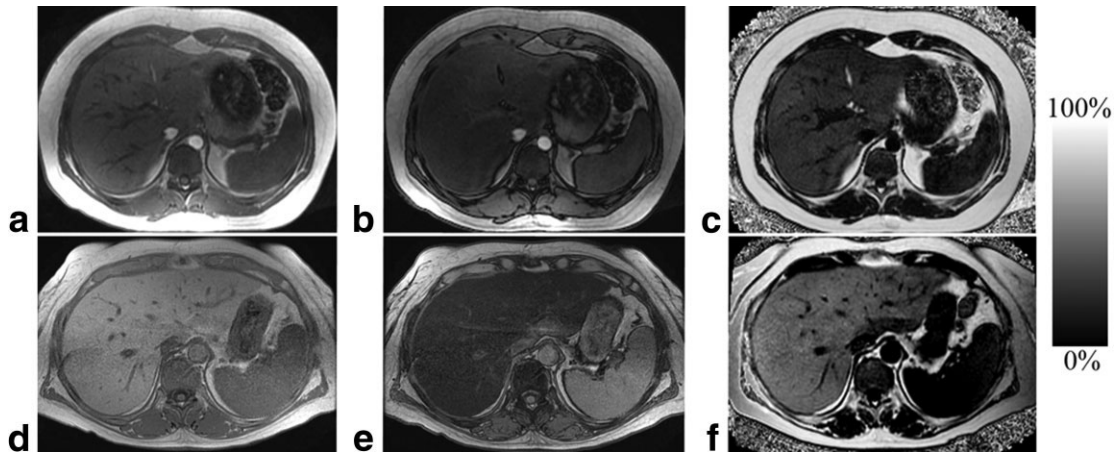

Figure 15. Hepatic steatosis is quantified utilizing IDEAL SPGR at 3T. In-phase images (**A,D**) and out-of-phase images (**B,E**) of two patients with fatty infiltration in the liver. Please note different signal intensity in the liver of the two patients in the R2* images from T_2*-IDEAL (**C,F**). The fat-signal fraction values in the liver of the patient in the upper row was 21% (C) as compared to more severe steatosis with 56% fat fraction in the patient in the lower row (F).

is achieved by producing an equilibrium magnetization that fluctuates from excitation to excitation (63). Hargreaves et al (59) proposed a single-point "phase sensitive" fat-water separation method that exploits the alternating phase behavior of SSFP images acquired with a passband width equal to the chemical shift between water and fat (eg, 210 Hz requiring TR = 4.6 msec at 1.5T) to ensure that the phase between water and fat are always in opposition. This group also proposed a dual-acquisition phase sensitive SSFP that separates fat and water by combining signal from two SSFP sequences that are added in quadrature and then phase corrected (64). Several other interesting methods have also been proposed (65–67), although a complete description is beyond the scope of this article.

Other fat suppression methods that are important for SSFP imaging, but do not specifically rely on SSFP's unique phase behavior, include the approach by Scheffler et al (61) that interrupts the steady state of the SSFP acquisition to play intermittent frequency selective fat saturation pulses. In addition, Reeder et al introduced a chemical shift-based water–fat separation method combined with SSFP that uniformly separates water from fat while being insensitive to B_0 inhomogeneities for cartilage imaging (69) and cardiac CINE imaging (40).

FAT QUANTIFICATION

The ability of chemical shift-based water–fat separation methods to accurately separate the signals from water and fat has led to great interest in quantifying fatty infiltration of organs in a variety of disease conditions, including nonalcoholic fatty liver disease (NAFLD). NAFLD is currently the leading cause of chronic liver disease in the US, affecting up to 34% of the US population (69,70). It is also related to the metabolic syndrome, which includes obesity and type II diabetes (69,71). The current gold standard for the diagnosis of NAFLD is liver biopsy, which is expensive, risky, and suffers from high sampling variability, greatly limiting its clinical utility. Therefore, there is a great need for noninvasive biomarkers such as imaging, not only for early detection of disease, but also to reliably quantify the severity of disease. Unfortunately, there are several confounding factors, such as T_1-related bias (5,55), noise-related bias (5), T_2* decay (47,55), and the complex spectrum of fat (54,55) that limits the ability of MRI to accurately quantify fat. The development of water–fat separation methods into a quantitative tool for measurement of fat is an active area of research by many groups (55,56,72–79) and may offer new perspectives in obesity research. Figure 15 shows examples of "fat-fraction" images acquired in two patients with steatosis using one approach (56).

CONCLUSION

Robust fat suppression methods are essential clinical tools necessary to improve the conspicuity of important anatomy and pathology, allowing MRI to fully exploit the utility of its intrinsically high soft-tissue contrast. Fortunately, there are a wide variety of fat suppression and water–fat separation methods available. The advantages, disadvantages, and suggested applications of most commonly used techniques for fat suppression and fat-water imaging are summarized in Table 1. Chemically selective methods work very well in many applications where good magnetic field homogeneity is present. Spatial-spectral pulses are used in specific clinical scenarios, such as cartilage imaging, again, when B_0 homogeneity is good. STIR imaging has been an excellent and robust conventional method that may, however, be replaced in the near future with chemical shift-based methods that are capable of robust fat suppression over large FOVs and in areas of severe magnetic field inhomogeneity. Chemical shift-based methods will likely play an increasing role for a wider variety of applications, particularly when scan time concerns are effectively addressed. Some of the newer techniques with chemical shift-based methods with accurate spectral modeling may provide continued improvement in the quality of fat suppression. Emerging fat quantification methods may become increasingly useful for quantification of disease severity such as hepatic steatosis and other disorders of abnormal fat deposition. Finally, utilizing nonuniform spectral response of different fat bands in SSFP, fat suppression methods have been introduced to various applications, and will help practitioners fully capitalize on the diagnostic utility of this important pulse sequence through improved suppression of fat.

REFERENCES

1. Machann J, Thamer C, Schnoedt B, et al. Standardized assessment of whole body adipose tissue topography by MRI. J Magn Reson Imaging 2005;21:455–462.
2. Armao D, Guyon JP, Firat Z, Brown MA, Semelka RC. Accurate quantification of visceral adipose tissue (VAT) using water-saturation MRI and computer segmentation: preliminary results. J Magn Reson Imaging 2006;23:736–741.
3. Li X, Youngren JF, Hyun B, et al. Technical evaluation of in vivo abdominal fat and IMCL quantification using MRI and MRSI at 3 T. Magn Reson Imaging 2008;26:188–197.
4. Kim H, Taksali SE, Dufour S, et al. Comparative MR study of hepatic fat quantification using single-voxel proton spectroscopy, two-point dixon and three-point IDEAL. Magn Reson Med 2008;59:521–527.
5. Liu CY, McKenzie CA, Yu H, Brittain JH, Reeder SB. Fat quantification with IDEAL gradient echo imaging: correction of bias from T(1) and noise. Magn Reson Med 2007;58:354–364.
6. Schuchmann S, Weigel C, Albrecht L, et al. Non-invasive quantification of hepatic fat fraction by fast 1.0, 1.5 and 3.0 T MR imaging. Eur J Radiol 2007;62:416–422.
7. Brix G, Heiland S, Bellemann ME, Koch T, Lorenz WJ. MR imaging of fat-containing tissues: valuation of two quantitative imaging techniques in comparison with localized proton spectroscopy. Magn Reson Imaging 1993;11:977–991.
8. Xiang QS, An L. Water-fat imaging with direct phase encoding. J Magn Reson Imaging 1997;7:1002–1015.
9. Rieke V, Butts Pauly K. MR thermometry. J Magn Reson Imaging 2008;27:376–390.
10. Haase A, Frahm J, Hanicke W, Matthaei D. 1H NMR chemical shift selective (CHESS) imaging. Phys Med Biol 1985;30:341–344.
11. Meyer CH, Pauly JM, Macovski A, Nishimura DG. Simultaneous spatial and spectral selective excitation. Magn Reson Med 1990;15:287–304.
12. Schick F. Simultaneous highly selective MR water and fat imaging using a simple new type of spectral-spatial excitation. Magn Reson Med 1998;40:194–202.

13. Star-Lack J, Vigneron DB, Pauly J, Kurhanewicz J, Nelson SJ. Improved solvent suppression and increased spatial excitation bandwidths for three-dimensional PRESS CSI using phase-compensating spectral/spatial spin-echo pulses. J Magn Reson Imaging 1997;7:745–757.
14. Schick F, Forster J, Machann J, Kuntz R, Claussen CD. Improved clinical echo-planar MRI using spatial-spectral excitation. J Magn Reson Imaging 1998;8:960–967.
15. Leong CS, Daniel BL, Herfkens RJ, et al. Characterization of breast lesion morphology with delayed 3DSSMT: an adjunct to dynamic breast MRI. J Magn Reson Imaging 2000;11:87–96.
16. Block W, Pauly J, Kerr A, Nishimura D. Consistent fat suppression with compensated spectral-spatial pulses. Magn Reson Med 1997; 38:198–206.
17. Schick F. Pulsed magnetization transfer contrast MRI by a sequence with water selective excitation. J Comput Assist Tomogr 1996;20:73–79.
18. Bieri O, Mamisch TC, Trattnig S, Kraff O, Ladd ME, Scheffler K. Optimized spectrally selective steady-state free precession sequences for cartilage imaging at ultra-high fields. Magma 2008;21: 87–94.
19. Nayak KS, Cunningham CH, Santos JM, Pauly JM. Real-time cardiac MRI at 3 Tesla. Magn Reson Med 2004;51:655–660.
20. Bydder GM, Pennock JM, Steiner RE, Khenia S, Payne JA, Young IR. The short TI inversion recovery sequence—an approach to MR imaging of the abdomen. Magn Reson Imaging 1985;3:251–254.
21. Bydder GM, Steiner RE, Blumgart LH, Khenia S, Young IR. MR imaging of the liver using short TI inversion recovery sequences. J Comput Assist Tomogr 1985;9:1084–1089.
22. Dousset M, Weissleder R, Hendrick RE, et al. Short TI inversion-recovery imaging of the liver: pulse-sequence optimization and comparison with spin-echo imaging. Radiology 1989;171:327–333.
23. Dixon WT. Simple proton spectroscopic imaging. Radiology 1984; 153:189–194.
24. Glover GH, Schneider E. Three-point Dixon technique for true water/fat decomposition with B0 inhomogeneity correction. Magn Reson Med 1991;18:371–383.
25. Ma J, Singh SK, Kumar AJ, Leeds NE, Broemeling LD. Method for efficient fast spin echo Dixon imaging. Magn Reson Med 2002;48: 1021–1027.
26. Reeder SB, Wen Z, Yu H, et al. Multicoil Dixon chemical species separation with an iterative least-squares estimation method. Magn Reson Med 2004;51:35–45.
27. Glover GH. Multipoint Dixon technique for water and fat proton and susceptibility imaging. J Magn Reson Imaging 1991;1:521–530.
28. Yu H, Reeder S, Shimakawa A, Gold G, Pelc N, Brittain J. Implementation and noise analysis of chemical shift correction for fast spin echo Dixon imaging. In: Proc 16th Annual Meeting ISMRM, Toronto; 2004. Abstract 2686.
29. Reeder SB, Pineda AR, Wen Z, et al. Iterative decomposition of water and fat with echo asymmetry and least-squares estimation (IDEAL): application with fast spin-echo imaging. Magn Reson Med 2005;54:636–644.
30. Pruessmann KP, Weiger M, Scheidegger MB, Boesiger P. SENSE: sensitivity encoding for fast MRI. Magn Reson Med 1999;42:952–962.
31. Sodickson DK, Manning WJ. Simultaneous acquisition of spatial harmonics (SMASH): fast imaging with radiofrequency coil arrays. Magn Reson Med 1997;38:591–603.
32. Ma J. Breath-hold water and fat imaging using a dual-echo two-point Dixon technique with an efficient and robust phase-correction algorithm. Magn Reson Med 2004;52:415–419.
33. Xiang Q, An L. Water-fat imaging with direct phase encoding. J Magn Reson Imaging 1997;7:1002–1015.
34. Yu H, Reeder SB, Shimakawa A, Brittain JH, Pelc NJ. Field map estimation with a region growing scheme for iterative 3-point water-fat decomposition. Magn Reson Med 2005;54:1032–1039.
35. Lu W, Hargreaves BA. Multiresolution field map estimation using golden section search for water-fat separation. Magn Reson Med 2008;60:236–244.
36. Xiang QS. Two-point water-fat imaging with partially-opposed-phase (POP) acquisition: an asymmetric Dixon method. Magn Reson Med 2006;56:572–584.
37. Ma J, Son JB, Bankson JA, Stafford RJ, Choi H, Ragan D. A fast spin echo two-point Dixon technique and its combination with sensitivity encoding for efficient T2-weighted imaging. Magn Reson Imaging 2005;23:977–982.
38. Jingfei M. Breath-hold water and fat imaging using a dual-echo two-point Dixon technique with an efficient and robust phase-correction algorithm. Magn Reson Med 2004;52:415–419.
39. Reeder SB, Hargreaves BA, Yu H, Brittain JH. Homodyne reconstruction and IDEAL water-fat decomposition. Magn Reson Med 2005;54:586–593.
40. Reeder SB, Markl M, Yu H, Hellinger JC, Herfkens RJ, Pelc NJ. Cardiac CINE imaging with IDEAL water-fat separation and steady-state free precession. J Magn Reson Imaging 2005;22:44–52.
41. Gold GE, Reeder SB, Yu H, et al. Articular cartilage of the knee: rapid three-dimensional MR imaging at 3.0 T with IDEAL balanced steady-state free precession—initial experience. Radiology 2006; 240:546–551.
42. Reeder SB, Yu H, Johnson JW, et al. T1- and T2-weighted fast spin-echo imaging of the brachial plexus and cervical spine with IDEAL water-fat separation. J Magn Reson Imaging 2006;24:825–832.
43. Reeder SB, McKenzie CA, Pineda AR, et al. Water-fat separation with IDEAL gradient-echo imaging. J Magn Reson Imaging 2007; 25:644–652.
44. Gerdes CM, Kijowski R, Reeder SB. IDEAL imaging of the musculoskeletal system: robust water fat separation for uniform fat suppression, marrow evaluation, and cartilage imaging. AJR Am J Roentgenol 2007;189:W284–291.
45. Siepmann DB, McGovern J, Brittain JH, Reeder SB. High-resolution 3D cartilage imaging with IDEAL SPGR at 3 T. AJR Am J Roentgenol 2007;189:1510–1515.
46. Pineda AR, Reeder SB, Wen Z, Pelc NJ. Cramer-Rao bounds for three-point decomposition of water and fat. Magn Reson Med 2005; 54:625–635.
47. Yu H, McKenzie CA, Shimakawa A, et al. Multiecho reconstruction for simultaneous water-fat decomposition and T2* estimation. J Magn Reson Imaging 2007;26:1153–1161.
48. Ma J, Bankson J, Stafford R. Multipoint Dixon imaging using sensitivity encoding. In: Proc 11th Annual Meeting ISMRM, Toronto; 2003. Abstract 1068.
49. McKenzie C, Reeder S, Shimakawa A, Pelc N, Brittain J. Abdominal three point Dixon imaging with self calibrating parallel MRI. In: Proc 12th Annual Meeting ISMRM, Kyoto; 2004. Abstract 917.
50. Reeder S, Vu A, Hargreaves B, et al. Rapid 3D-SPGR imaging of the liver with multi-echo IDEAL. In: Proc 14th Annual Meeting ISMRM, Seattle; 2006. Abstract 2444.
51. Ma J, Choi H, Stafford RJ, Miller MJ. Silicone-specific imaging using an inversion-recovery-prepared fast three-point Dixon technique. J Magn Reson Imaging 2004;19:298–302.
52. Levin YS, Mayer D, Yen YF, Hurd RE, Spielman DM. Optimization of fast spiral chemical shift imaging using least squares reconstruction: application for hyperpolarized (13)C metabolic imaging. Magn Reson Med 2007;58:245–252.
53. Reeder SB, Brittain JH, Grist TM, Yen YF. Least-squares chemical shift separation for (13)C metabolic imaging. J Magn Reson Imaging 2007;26:1145–1152.
54. Yu H, Shimakawa A, McKenzie CA, Brodsky E, Brittain JH, Reeder SB. Multiecho water-fat separation and simultaneous R2* estimation with multifrequency fat spectrum modeling. Magn Reson Med. 2008 Nov;60(5):1122–34.
55. Bydder M, Yokoo T, Hamilton G, et al. Relaxation effects in the quantification of fat using gradient echo imaging. Magn Reson Imaging 2008;26:347–359.
56. Reeder SB, Robson PM, Yu H, Shimakawa A, Hines CD, McKenzie CA, Brittain JH. Quantification of hepatic steatosis with MRI: the effects of accurate fat spectral modeling. J Magn Reson Imaging. 2009 Jun;29(6):1332–9.
57. Ma J. Dixon techniques for water and fat imaging. J Magn Reson Imaging 2008;28:543–558.
58. Sekihara K. Steady-state magnetizations in rapid NMR imaging using small flip angles and short repetition intervals. IEEE Trans Med Imaging 1987;6:157–164.
59. Hargreaves BA, Vasanawala SS, Nayak KS, Hu BS, Nishimura DG. Fat-suppressed steady-state free precession imaging using phase detection. Magn Reson Med 2003;50:210–213.
60. Scheffler K, Heid O, Hennig J. Magnetization preparation during the steady state: fat-saturated 3D TrueFISP. Magn Reson Med 2001;45:1075–1080.

61. Vasanawala SS, Pauly JM, Nishimura DG. Linear combination steady-state free precession MRI. Magn Reson Med 2000;43:82–90.
62. Vasanawala SS, Hargreaves BA, Pauly JM, Nishimura DG, Beaulieu CF, Gold GE. Rapid musculoskeletal MRI with phase-sensitive steady-state free precession: comparison with routine knee MRI. AJR Am J Roentgenol 2005;184:1450–1455.
63. Vasanawala SS, Pauly JM, Nishimura DG. Fluctuating equilibrium MRI. Magn Reson Med 1999;42:876–883.
64. Hargreaves BA, Bangerter NK, Shimakawa A, Vasanawala SS, Brittain JH, Nishimura DG. Dual-acquisition phase-sensitive fat-water separation using balanced steady-state free precession. Magn Reson Imaging 2006;24:113–122.
65. Leupold J, Hennig J, Scheffler K. Alternating repetition time balanced steady state free precession. Magn Reson Med 2006;55:557–565.
66. Lu A, Grist TM, Block WF. Fat/water separation in single acquisition steady-state free precession using multiple echo radial trajectories. Magn Reson Med 2005;54:1051–1057.
67. Lu A, Brodsky E, Grist TM, Block WF. Rapid fat-suppressed isotropic steady-state free precession imaging using true 3D multiple-half-echo projection reconstruction. Magn Reson Med 2005;53:692–699.
68. Reeder SB, Pelc NJ, Alley MT, Gold GE. Rapid MR imaging of articular cartilage with steady-state free precession and multipoint fat-water separation. AJR Am J Roentgenol 2003;180:357–362.
69. Chitturi S, Abeygunasekera S, Farrell GC, et al. NASH and insulin resistance: insulin hypersecretion and specific association with the insulin resistance syndrome. Hepatology 2002;35:373–379.
70. Harrison SA, Neuschwander-Tetri BA. Nonalcoholic fatty liver disease and nonalcoholic steatohepatitis. Clin Liver Dis 2004;8:861–879, ix.
71. Marchesini G, Brizi M, Bianchi G, et al. Nonalcoholic fatty liver disease: a feature of the metabolic syndrome. Diabetes 2001;50:1844–1850.
72. Yokoo T, Bydder M, Hamilton G, et al. Hepatic fat quantification by low flip-angle multi-echo gradient-echo MR imaging: a clinical study with validation with MR spectroscopy. In: Proc 16th Annual Meeting ISMRM, Toronto; 2008. Abstract 706.
73. Gard CD, Warner TF, Yu H, et al. Quantification of hepatic steatosis with MRI: validation in the Ob/ob Mouse at 3T. In: Proc 16th Annual Meeting ISMRM, Toronto; 2008. Abstract 707.
74. Altbach MI, Li Z, Squire SW, et al. Rapid T2 and lipid-water imaging of the liver with radial IDEAL GRASE. In: Proc 16th Annual Meeting ISMRM, Toronto; 2008. Abstract 708.
75. Sugay S, Bydder M, Yokoo T, et al. Fat quantification using SPIO as a surrogate marker for iron accumulation in the liver. In: Proc 16th Annual Meeting ISMRM, Toronto; 2008. Abstract 711.
76. Cavassila S, Bucur A, Ratiney H, Cudalbu C, Beuf O, Pilleul F. Quantification of the hepatic fatty infiltration and the metabolite concentrations using magnetic resonance spectroscopy and in and out of phase imaging. In: Proc 16th Annual Meeting ISMRM, Toronto; 2008. Abstract 712.
77. Hussain HK, Oral EA, Rohrer S, et al. Validation of hepatic fat quantified on 3T MRI via histopathologic correlation in patients with non-alcoholic steatohepatitis. In: Proc 16th Annual Meeting ISMRM, Toronto; 2008. Abstract 713.
78. Morell G, Hopkins P, Taylor J. High resolution measurement of hepatic fat volume fraction in a single breathhold. In: Proc 16th Annual Meeting ISMRM, Toronto; 2008. Abstract 2702.
79. Sommer G, Ludwig U, Baumann T, Paul D. Intrinsic water-suppression in TIDE-bSSFP applied for quantification and differentiation of adipose tissue. In: Proc 16th Annual Meeting ISMRM, Toronto; 2008. Abstract 2703.